International Journal of Nanoelectronics and Materials
Volume 14 (Special Issue) August 2021 [59-68]

Electromagnetic Torque Performance Evaluation of Concentric Magnetic Gear Alternative Conditions using Finite Element

M. F. M. A. Halim[1,2*], E. Sulaiman[1], R. Aziz[1], S. Othman. S. M. Naufal[1] A. A Rahman[2] and T. Kosaka[3]

[1]Research Center for Applied Electromagnetics, Institute of Integrated Engineering, Universiti Tun Hussein Onn Malaysia
[2]Centre for Robotics & Industrial Automation, Fakulti Teknologi Kejuruteraan Elektrik & Elektronik Universiti Teknikal Malaysia Melaka, Malaysia
[3]Nagoya Institute of Technology, Japan.

Corresponding Author's Email: mohd.firdaus@utem.edu.my

ABSTRACT

Concentric magnetic gear(CMG) research mainly focuses on the CMG act as torque increaser and with stationary pole piece condition. Yet, technically CMG can be designed as speed increaser gear with the alternative rotating condition. This paper investigates an initial torque performance of CMG in alternative conditions operating as torque increaser and speed increaser gear. The conditions are when either the inner pole pair or outer pole pair is set stationary while the pole piece component act as rotors. The structure and working principle of the motor are described in detail. The torque performance from finite element software, JMAG Designer 16.0 simulation, as compared with the conventional condition and discussed briefly. The result showed that the conventional condition generates a minor percentage of torque ripple at 1.52%. The highest gear ratio is achieved when the pole piece serves as the outer rotor. Abnormality was also discovered in the conventional condition when the gear operates as a speed increaser. This study concludes that the CMG functions better as a torque increaser instead of a speed increaser gear.

Keywords: Finite element, flux modulation, magnetic gear, torque increaser

1. INTRODUCTION

Magnetic gear (MG) is still uncommon if compared to mechanical gears, even though it can offer better features like contactless torque transmission, low maintenance cost, and low noise [1-6]. The main reason for this situation is that MG usage requires significant system application changes, for example, in a combustion engine vehicle where chain and sprocket have to be removed, and chassis has to be modified. However, for high-end application such as part of an aerospace system, MG was developed and studied extensively. The study of MG in the aerospace application was driven by NASA strategic plan to produce low cost, environmentally friendly, small aircraft for emerging markets such as the short-haul category [7-9]. MG is also planned to be used in down borehole oil and gas pumping applications. It inherently protects against overloads by a harmlessly slipping mechanism if an overload torque is applied automatically and safely re-engaged when the faulty torque is identified and removed [10].

Several magnetic gear designs were proposed in the past fifty years. The general concept was to replace the teeth and slots of mechanical gears with the North (N)-poles and South (S)-poles of permanent magnets (PMs). The development of an effective MG was very challenging, mainly due to the unavailability of finite element software. Figure 1 (a-d) shows the structure of magnetic gear in the late 19th century. At the end of the 19th century, with

the discovery of rare–earth Neodymium-Iron-boron (NdFeB) PMs, new hope ignited among machine designer.

The most important design was in the early 2000s, where [11-13] managed to realize high torque density MG using flux modulation principle comparable to the mechanical gear torque density. Figure 2 shows the concentric MG structure that uses the flux modulation principle to transfer torque from the inner rotor to the outer rotor. The development of an effective MG was very challenging, mainly due to the unavailability of finite element software.

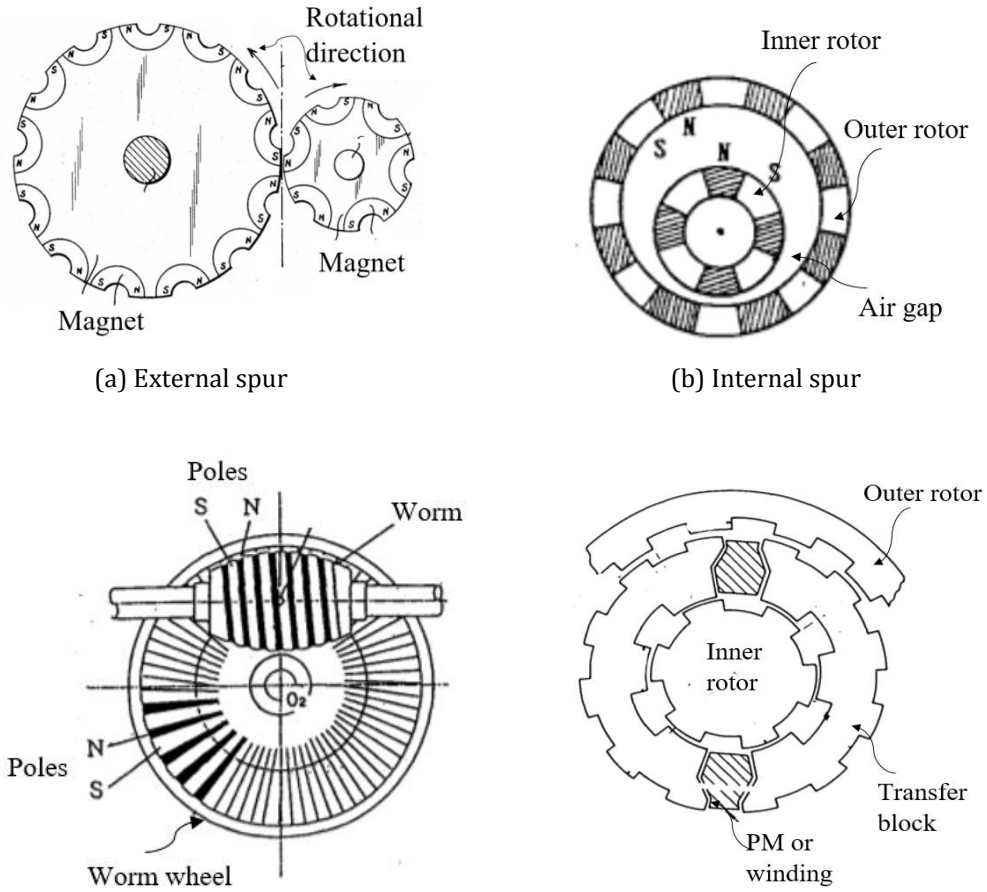

(a) External spur (b) Internal spur

(c) Worm magnetic gear (d) Reluctance magnetic gear

Figure 1. Structure of magnetic gear in early days.

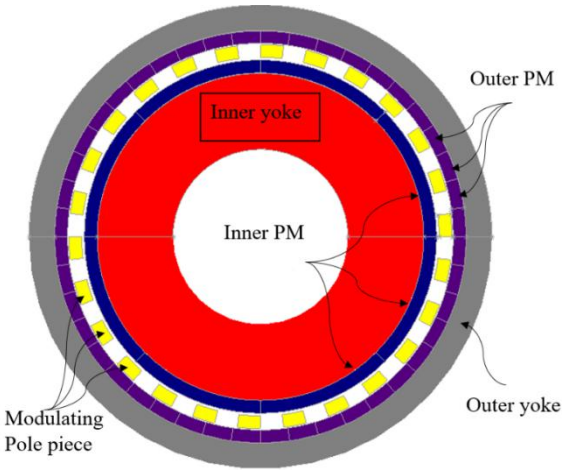

Figure 2. Structure of CMG.

CMG consists of three main components, namely inner pole pair, pole piece, and outer pole pair. The inner rotor consists of a surface-mount permanent magnet (PM) and rotor yoke. The modulating pole piece is soft magnetic material placed between the inner rotor and the outer rotor. The outer rotor is made similar to the inner rotor but at an external location. The inner rotor shaft is connected to the prime-mover while the outer rotor is connected to the output. The modulating pole piece is stationary. This setup has been explored extensively in many publications [14-18]. However, many studies only focus on the gear operating as torque increaser when the modulating pole piece (FMP) is in a stationary condition. In this paper, three-rotor rotation setting conditions of CMG were analyzed when it operates as torque increase and speed increase. The requirements are when either the inner pole pair or outer pole pair is set stationary while the pole piece component act as rotors. The structure and working principle of the motor are introduced in detail. The torque performance from the simulation was compared and discussed. JMAG Designer version 16.0 was used for this study. The study is meant to assess the MG performance in different conditions, based on torque behavior, torque ripple, torque density and power delivery.

2. RESEARCH METHODOLOGY

2.1 Working Principle of CMG

The relationship between inner pole pair p_h, outer pole pair p_l, and the number of modulating pole piece n_s can be written as

$$n_s = p_h + p_l \tag{1}$$

The FMP creates space harmonic flux density at the inner and outer air gap. The rotational velocity flux density harmonic produced by the inner rotor is given by

$$w_l = \frac{p_h}{p_h - n_s} w_h \tag{2}$$

where w_l is the rotational velocity of the flux density space harmonic of the outer pole pair and w_h is the rotational velocity of the inner rotor. Then the gear ratio G_r is written as

$$G_r = \frac{w_h}{w_l} = -\frac{p_l}{p_h} \tag{3}$$

The negative sign indicates that both pole pair rotates in a different direction. This gear ratio holds for the condition where the FMP remains stationary, $w_p = 0$. If each term in (1) is multiplied by its respective rotational velocity, the fundamental equation to determine the gear ratio according to each condition is

$$w_l p_l + w_h p_h = w_p n_p \tag{4}$$

Hence, the gear ratio when the inner pole pair is held stationary and when the outer pole pair is held stationary can be expressed as

$$G_r = \frac{w_l}{w_p} = \frac{n_p}{p_l} \quad , w_h = 0 \tag{5}$$

$$G_r = \frac{w_h}{w_p} = \frac{n_p}{p_h} \quad , w_l = 0 \tag{6}$$

Equation (5) and (6) present the magnetic gear having a reluctance type outer rotor, which has an inherent firm structure [19]. The positive sign indicates that both pole pair rotates in the same direction. The input and output torques of the gear are equivalent to the inner and outer rotor torque. When the inner pole pair is set to stationary, the pole piece becomes the new inner rotor, and the outer pole pair remains as an outer rotor. Equation (5) is rewritten as

$$G_{rnew} = \frac{w_p}{w_l} = \frac{p_l}{n_p} \quad ,w_h = 0 \tag{7}$$

Another important characteristic in gear ratio selection is that for gear to function as torque increaser gear, $p_h > p_l$ while for speed increaser, $p_h < p_l$ [20-21].

2.2 Simulation Configuration

Two main structures are constructed using JMAG to demonstrate the condition mentioned earlier. Designer 16.0. Each design represents torque increaser type gear where $p_h > p_l$ and speed increaser type gear where $p_h < p_l$. The condition for each type is set according to the equation given in (3), (6), and (7). The torque waveform, average torque, power density, and torque ripple were evaluated for each setup. Table 1 displays the design specification of the CMG used in the simulation. Figure 3(a) and (b), on the other hand, illustrate the structure used in this study. The material selected for PM is Neodymium Iron boron (NdFeb) with a remanence of 1.2T, whilst the material chosen for the inner yoke, outer yoke, and modulating pole piece is NSSMC 35H210 with a maximum flux density of 1.7T.

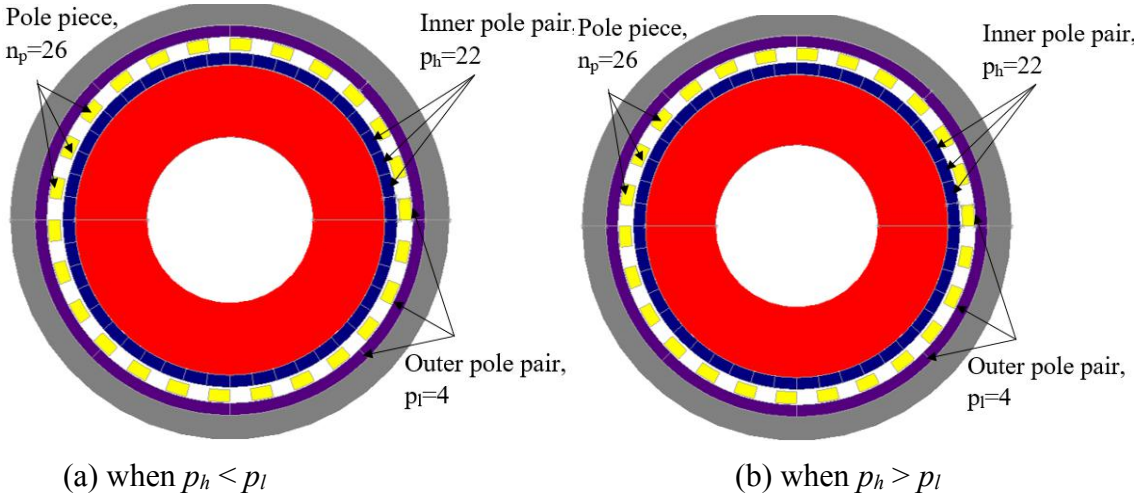

Figure 3. Structure of flux modulation concentric magnetic gear, **(a)** when $p_h < p_l$ and **(b)** when $p_h > p_l$.

Table 1. Specification of Concentric MG used in the simulation

Parameters	$p_h > p_l$	$p_h < p_l$
Inner pole pair, p_h	4	22
Outer pole pair, p_l	22	4
Pole piece, n_p	26	26
Inner air gap	1mm	1mm
Outer air gap	0.5mm	0.5mm
Overall diameter	180mm	180mm
Stack length	30mm	30mm
Gear ratio eq. (3)	5.50	0.18
Gear ratio eq. (5.1)	0.846	0.15
Gear ratio eq. (6)	6.50	1.18
Volume	6.2×10^{-4} m^3	

In the transient magnetic analysis, the rotor is set to rotate based on the gear ratio for each condition shown in Table 2.

Table 2. Rotor rotation setting based on conditions

Condition/Structure	$p_h > p_l$	$p_h < p_l$
	Rotation (rpm)	
n_p =0		
inner rotor	1100	200
outer rotor	200	1100
$w_h = 0$		
inner rotor	1100	200
outer rotor	1300	1300

$w_l = 0$		
inner rotor	1300	1100
outer rotor	200	1300

3. RESULTS AND DISCUSSION

The rotors rotation direction is opposite to each other in (3). The simulation is set for ¼ period or 90°. Figure 3(a) to Figure 3(c) shows the torque waveform according to the torque increaser condition. Figure 4(a) to Figure 4(c) shows the torque waveform according to the speed increaser condition.

In Figure 4(a), Figure 4(c), Figure 5(a) and Figure 5(c), the inner rotor torque is always in the negative region. In this simulation, negative torque means that the external force of that value is required to move the inner rotor. The positive torque is the torque developed from the interaction and alignment of the magnetic poles of the p_l, p_h, *and* n_p. Contrary to the above condition, the torque waveforms in Figure 4(b) and Figure 5(b) at the inner rotor was positive while the outer rotor was opposing. It is because the pole piece delivered the outer rotor torque. Figure 5(a) produces the trending of inner rotor torque. At a more extended period, the torque may reach zero and stall. Similar behavior was also discovered in the previous publication [22]. Table 3 summarizes the result of all the conditions.

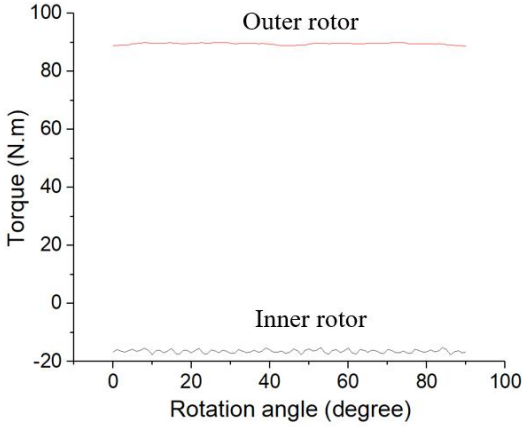

(a) Speed 1100:200

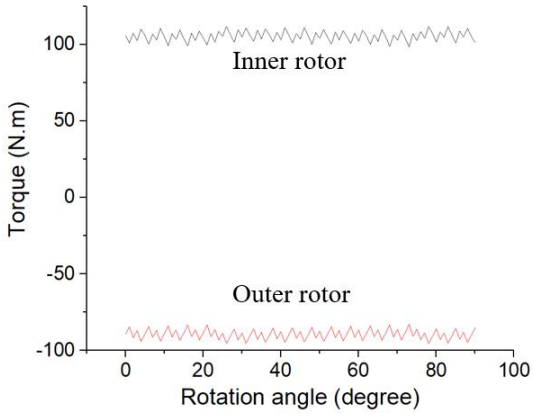

(b) Speed 1100:1300

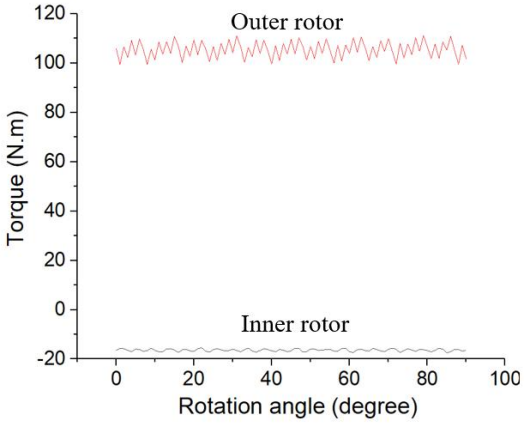

(c) Speed 1300:200

Figure 4(a)-(c). Torque waveform simulated on torque increaser gear design according to the condition in Table 2.

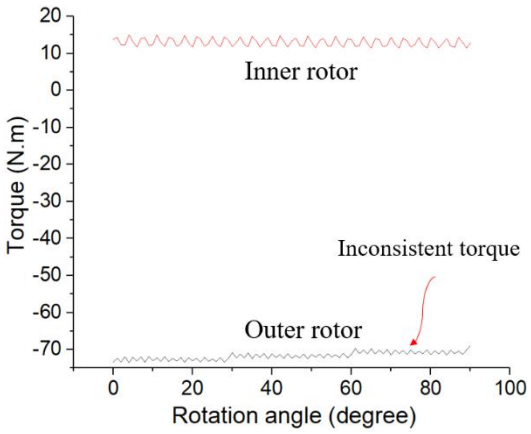

(a) Speed 200:1100

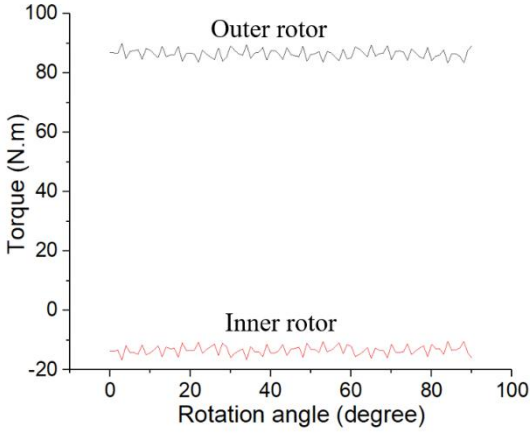

(b) Speed 200:1300

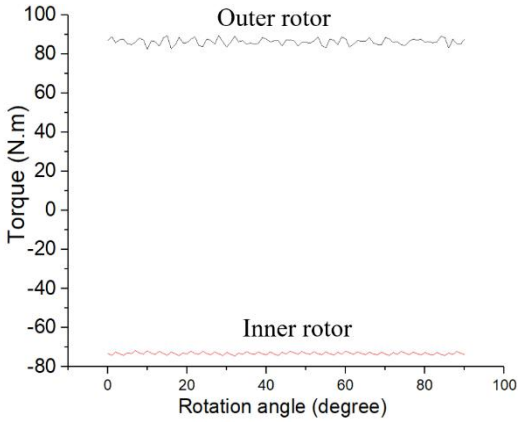

(c) Speed 1100:1300

Figure 5(a)-(c). Torque waveform simulated on speed increaser gear design according to the condition in Table 2.

Table 3. Simulation result torque analysis in 6 conditions.

Structure	Condition	Average Torque (N.m)		Torque ripple (%)		Power (kW)	Power density (kW/m^3)	Gear ratio
		Inner rotor	Outer rotor	Inner rotor	Outer rotor			
$p_h > p_l$	$w_p = 0$	16.40	89.53	15.72	1.52	18	3021	5.50
	$w_h = 0$	105.53	89.38	12.72	14.14	116	19610	0.84
	$w_l = 0$	16.38	105.53	12.59	11.10	21	3561	6.50
$p_h < p_l$	$w_p = 0$	71.66	13.01	6.48	27.58	14	2415	0.18
	$w_h = 0$	86.48	13.30	7.61	47.06	17	2917	0.15
	$w_l = 0$	73.11	86.41	3.82	8.29	95	16040	1.18

The highest average outer torque of 105.53N.m and 86.41N.m were produced when $w_l=0$ for $p_h > p_l$ and $p_h < p_l$ structure. It occurs when the pole piece act as the outer rotor. The smallest torque, on the other hand, ripple at the outer rotor of 1.52% occurs when $w_p = 0$ for $p_h > p_l$

structure. In $p_h < p_l$, the smallest torque ripple happens when $w_l=0$. The highest power density of 19610kW/m^3 was produced when $w_h=0$ for $p_h > p_l$, but for $p_h < p_l$, it occurred when $w_l=0$. The primary variable in power density calculation is the rotational speed, which is why the smallest gear ratio in $p_h > p_l$ and the most significant gear ratio in $p_h < p_l$ has the highest power density in each structure. The highest gear ratio of "6.5" was when $w_l=0$ *in* $p_h > p_l$. The smallest gear ratio, "0.15", indicates a speed increaser gear. The gear ratio also changed in both structures as the condition change. An initially torque increaser MG structure $p_h > p_l$ became speed increaser gear when $w_h=0$, while the initially speed increaser gear structure will be changed to torque increaser when $w_l=0$. Overall, the finite element result conforms to the gear ratio calculated at different condition, which was initially presented in equation (3), (6), and (7) except for $p_h < p_l$ when $w_p = 0$ that is CMG can be designed in an alternative condition which produces a steady-state torque at different gear ratio. The validity of this condition will have to be verified through fabrication and lab testing in the future.

4. CONCLUSION

Concentric magnetic gear can produce additional two conditions that yield two gear ratios from the same structure. This paper explores different possible situations that can be tested on this structure when $p_h < p_l$. Three conditions were proposed and discussed. Two structures were designed and evaluated using a finite element. The result concludes that:
When $p_h > p_l$, CMG can produce a lower torque ripple, higher average torque, higher gear ratio and higher power density than on the structure when $p_h < p_l$. This result proves that CMG works better when $p_h > p_l$. This finding also indicates that CMG cannot operate as a speed increaser when $p_h < p_l$ at $w_p = 0$. This paper also concludes that five working conditions can be used on CMG topology to produce different gear ratio.

ACKNOWLEDGEMENTS

Many thanks to the Universiti Tun Hussein Onn Malaysia (UTHM) and Universiti Teknikal Malaysia Melaka (UTeM). This work was supported by the Tier 1 Research Grant H755, UTHM

REFERENCES

[1] K. Aiso, K. Akatsu, and Y. Aoyama, Reluctance magnetic gear and flux switching magnetic gear for high speed motor system, 2017 IEEE Energy Convers. Congr. Expo. ECCE (2017) 2445–2452.

[2] B. Mcgilton, P. M. Mueller, and A. Mcdonald, Review of Magnetic Gear Technologies and their Applications in Marine Energy, 5th IET International Conference on Renewable Power Generation (RPG) (2016) 1–6.

[3] M. Chen, K. T. Chau, W. Li, C. Liu, and C. Qiu, Design and analysis of a new magnetic gear with multiple gear ratios, IEEE Trans. Appl. Supercond., **24**, 3 (2014) 1–4.

[4] E. Park, C. Gim, S. Jung, and Y. Kim, A gear efficiency improvement in magnetic gear by eddy-current loss reduction, Int. J. Appl. Electromagn. Mech., **1** (2018) 1–10.

[5] A. Al Faysal and S. M. Haris, Development of Magnetic Gears: A Review, J. Kejuruter., **1**, 7 (2019) 49–56.

[6] L. Xianglin, C. K. T., C. Ming, H. Wei, and D. Yi, A New Coaxial Magnetic Gear Using Stationary Permanent Magnet Ring, International Conference on Electrical Machines and Systems (2013) 634–638.

[7] J. L. Perez-Diaz, E. Diez-Jimenez, M. A. Alvarez-Valenzuela, J. Sanchez-García-Casarrubios, C. Cristache, and I. Valiente-Blanco, Magnetic Gearboxes for Aerospace Applications, Aerosp. Mech. Symp. (2014) 365–374.

[8] F. T. Thomas, S. Justin J, and A. C. Zachary, Electromagnetic Mass and Efficiency of Magnetic Gears for Electrified Aircraft, 2019 AIAA/IEEE Electr. Aircr. Technol. Symp. (2019) 1–25.
[9] V. M. Asnani and T. F. Tallerico, NASA' s Magnetic Gearing Research for Electrified Aircraft, 2018 AIAA/IEEE Electric Aircraft Technologies Symposium (EATS) (2018) 1–12.
[10] Daleel, Magnomatics announce exclusive partnership with Zilift, Magnomatics Ltd, 2015. https://www.scmdaleel.com/article/magnomatics-announce-exclusive-partnership-with-zilift/83.
[11] K. Atallah, S. D. Calverley, and D. Howe, High-performance magnetic gears, J. Magn. Magn. Mater. **272-276** (2004) 1727-1729.
[12] K. A. and D. Howe, A novel high-performance linear magnetic gear, IEEE Trans. Magn. **37**, 4 (2001) 2844–2846.
[13] S. D. C. and D. H. K. Atallah, Design, analysis and realization of a high- performance magnetic gear, IEE Proceedings-Electric Power Appl. **150**, 2 (2004) 139–145.
[14] B. McGilton, R. Crozier, and M. Mueller, Optimization procedure for designing a magnetic gear, J. Eng. **13** (2017) 840–843.
[15] X. Zhang, X. Liu, C. Wang, and Z. Chen, Analysis and Design Optimization of a Coaxial Surface-Mounted Permanent-Magnet Magnetic Gear, Energies **7** (2014) 8535–8553.
[16] M. Chen, K. T. Chau, W. Li, and C. Liu, Cost-effectiveness comparison of coaxial magnetic gears with different magnet materials, IEEE Trans. Magn. **50**, 2 (2014) 821–824.
[17] Y. J. Ge, C. Y. Nie, and Q. Xin, A three dimensional analytical calculation of the air-gap magnetic field and torque of coaxial magnetic gears, Prog. Electromagn. Res. **131** (2012) 391–407.
[18] C. S. Gim, E. J. Park, S. Y. Jung, and Y. J. Kim, Torque Characteristic Analysis of Coaxial Magnetic Gear According to Fillet Parameter of Pole Piece, ICEMS 2018 - 2018 21st Int. Conf. Electr. Mach. Syst. **1** (2018) 2557–2560.
[19] X. Wang, R. Nie, H. Chen, H. Wang, and T. Xu, Electromagnetic analysis and optimization for a dual-rotor switched reluctance machine, J. Magn. **24**, 2 (2019) 342–349.
[20] M. F. M. A. Halim, E. Sulaiman, and R. N. F. K. R. Othman, Flux modulated rotating pole piece magnetic gear, Int. J. Power Electron. Drive Syst **11**, 4 (2020) 1731–1736.
[21] M. F. Mohd Ab Halim, E. Sulaiman, R. N. F. K. R. Othman, and A. A. Rahman, A new speed multiplier coaxial magnetic gear, Prog. Electromagn. Res. M **93** (2020) 145-154.
[22] C. V. Pop and D. Fodorean, In-Wheel Motor with Integrated Magnetic Gear for Extended Speed Applications, 2016 Int. Symp. Power Electron. Electr. Drives, Autom. Motion **1143**, (2016) 413–418.